



Combining ZnO inverse opal and ZnO nanorods using ALD and hydrothermal growth

Dániel Karajz¹ · Domonkos Cseh¹ · Bence Parditka² · Zoltán Erdélyi² · Imre Szilágyi¹

Received: 19 January 2022 / Accepted: 30 January 2022
© The Author(s) 2022

Abstract

In this paper, we combine the atomic layer deposition synthesis method of inverse opal with the hydrothermal growth of nanorods. From 460 nm polystyrene nanospheres opal crystals were produced using vertical deposition on Si wafers. The opal templates were covered with ZnO by atomic layer deposition. High temperature annealing was used to remove the polystyrene nanospheres to obtain the inverse opal structure. For the hydrothermal growth of ZnO nanorods, two production routes were analysed: hydrothermal reaction before and after the removal of the template. The two paths produced two distinct structures, one with plate like formations and one with nanorods, respectively. Also, the sample modified by the hydrothermal growth after the annealing showed slight differences in optical properties compared to the regular inverse opal. Morphology, composition and structure of the samples were explored using SEM, EDX and XRD. Optical properties were investigated with reflectance UV–Vis spectroscopy. Thermal stability of the polystyrene opal was determined using TG.

Keywords Inverse opal · Atomic layer deposition · Hydrothermal growth · Nanorods

Introduction

Inverse opal structured materials are known and researched for their optical properties; the photonic band gap, which prevent the propagation of light at certain frequencies and the “slow” photon effect, what can cause an absorbance enhancement at the borders of the photonic band gap [1–3]. These properties can be utilized in optical related fields like photocatalysis [4, 5], photoelectrochemistry [6, 7], photosensors [8] or optical devices [9]. Inverse opal photonic crystals are easy to be manufactured using the bottom-up building. Various techniques can be applied, that exploits the self-assembly of colloid nanoparticles to build up 3D

nanostructures using nanospheres [10, 11] and several infiltration methods can be used to fill up the voids of the colloid crystal, such as sol–gel technique [12], CVD (chemical vapour deposition) [13], electrodeposition [14] and ALD (atomic layer deposition) [15–17]. ALD is excellent method for the coating of structures with high aspect ratio, like opal crystals, which is due to its cyclical, surface controlled and self-limited operation [18]. The choice of the material of inverse opals, it depends on the aim of the product, but for photocatalytic purposes TiO₂ is advantageous, ZnO is also similarly beneficial [19, 20]. The position of the photonic band gap in the spectrum of light depends on mainly two variables: the size of the air voids in the structure and the refractive index of the crystal material [21].

One-dimensional nanostructures like nanorods can be advantageous in fields where its high aspect ratio can be exploited like sensing or photocatalysis [22, 23], and in these fields, ZnO nanorods are vastly researched [24]. Several techniques are capable to synthesize metal oxide nanorods, like ZnO: electrospinning [24], MOCVD (metal organic chemical vapour deposition) [25], chemical bath deposition [26] and hydrothermal synthesis [27] to name a few. During hydrothermal deposition the final shape, size, quantity and surface density of the ZnO nanostructures can be affected by the parameters of the synthesis such as the concentration

✉ Dániel Karajz
karda412@gmail.com

✉ Imre Szilágyi
szilagyi.imre.miklos@vbk.bme.hu

¹ Department of Inorganic and Analytical Chemistry, Faculty of Chemical Technology and Biotechnology, Budapest University of Technology and Economics, 1111 Műegyetem rkp. 3., Budapest, Hungary

² Department of Solid State Physics, Faculty of Sciences and Technology, University of Debrecen, P.O. Box 400, 4002 Debrecen, Hungary

and type of the growth solution, temperature, reaction time, pH, seed layer and usage of capping agents [28]. ALD and hydrothermal methods are regularly used together to grow nanorods on the surface of structures. Usually ALD provides a layer where the growth of the rods can start and this layer is named as seed layer [29–31].

Inverse opal photonic crystals can be combined with other nanostructures: e.g. with nanospheres [32, 33], hydrothermally grown nanowires/rods [34, 35], also carbon nanotubes can be incorporated into the structure [36, 37]. For higher dimensional structures inverse opals can be filled e.g. with reduced graphene oxide [38]; furthermore, inverse opals with different sized void holes can be prepared [39]. It was also reported that TiO₂ inverse opal were combined with ZnO nanorods to boost the light harvesting capability of the nanorods and to increase the surface area of the structure [34]. Pure ZnO inverse opal and nanorod structure hybrid was synthesized with thin nanorods grown inside the inverse opal coated with TiO₂ was researched [40]. Interesting direction is that instead of filling the opal structure, a seed layer is deposited to help the growth of the nanorods, making a nanorod network in shape of an inverse opal [41]. Looking at the beforementioned literature, pure ZnO inverse opal/nanorod hybrids were not synthesized and the possible effect of the nanorods on the optical properties were not investigated earlier.

In this study, the synthesis of ZnO inverse opals were done by using vertical deposition and atomic layer deposition. ZnO nanorods were grown on this backbone structure using hydrothermal synthesis method. The hydrothermal synthesis was done before and after the annealing step of the inverse opal preparation, meaning before and after the removal of the sacrificial polystyrene nanosphere templates. Our aim is to explore the hybrid structure and its optical properties. The polystyrene nanospheres were tested using thermogravimetry to check their suitable annealing temperature. The inverse opal, nanorods and the hybrid structures were studied by SEM–EDX (scanning electron microscopy—energy dispersive X-ray microanalysis) and XRD (X-ray diffraction). The optical properties were investigated by UV–Vis spectroscopy.

Materials and methods

Preparation of the colloid crystals

Opal crystal templates were synthesized by vertical deposition similar to the method our researched group used in an earlier article [42]. 460 nm diameter polystyrene nanospheres (Sigma Aldrich) were received in the form of 10 w/w% water suspension, which was diluted to a 0.3 w/w% suspension and ultrasonicated for 2 h. In the meantime, Si

substrates were sliced to make roughly 1 × 3 cm slides, these slides were cleaned with soap, then ethanol and distilled water, finally treated with “piranha” solution (3:1 mixture of concentrated sulfuric acid and 30% hydrogen-peroxide) for 1 h. For the vertical deposition the slide was put in vertically in the suspension and got heat treated in a Nabertherm L9/11/B410 furnace with the following heat program: 40 h at 50 °C, then 6 h at 80 °C. During vertical deposition a large glass beaker filled with water was inside the furnace, as higher humidity in the furnace reduced the cracks of the opal crystal [43].

Hydrothermal growth of the nanorods

The hydrothermal procedure was executed using a stainless-steel autoclave with a 50 mL Teflon inlet. For the growth solution 2.5 mmol zinc-acetate (Sigma Aldrich) and hexamethylene-tetramine (Sigma Aldrich) were dissolved in 50 mL water, then filled into the Teflon inlet. The slide sample was fixed with a rubber ring to allow the ZnO layer and the inverse opal film to face the bottom of the inlet; this way the sample could be separated from the precipitate easier. The reaction was done at 90 °C for 3 h in a Nabertherm L9/11/B410 furnace, then the sample was rinsed with distilled water and dried at 50 °C for 30 min. This recipe is based on a recent article [28]. The ZnO nanorods were both grown on ZnO coated reference Si wafers and on the top of the inverse opals.

Atomic layer deposition

ZnO layer deposition was carried out with a Beneq TFS-200-186 flow ALD reactor using DEZ (diethylzinc) and water as precursors. The deposition was carried out at 50 °C and 1.4 mbar in the reactor and 7 mbar in the outer chamber, the pulse time was 300 ms and the purge time was 3 s. 434 cycles were done, corresponding to a ZnO film thickness of about 36 nm. The 36 nm layer thickness is equal to the smallest hole in an inverse opal made out of 460 nm polystyrene nanospheres, and this is due to the hexagonal structure of the opal. For hexagonal structure the smallest hole is in the [1 1 1] planes, which hole is equal to the 7.75% of the sphere diameter and that is around 36 nm [15]. Apart from the coating of the opal templates, Si wafers were coated as well to serve as reference and seeding layer for the ZnO hydrothermal growth for the reference nanorod forest.

Inverse opal samples

Removal of the polystyrene nanospheres was done in the Nabertherm L9/11/B410 furnace. The coated opals were annealed with the following heat program: the furnace was

heated up to 500 °C under 4 h, then kept at this temperature for 2 h. The polystyrene nanospheres were removed from the inverse opal structure after the hydrothermal growth of the nanorods in one sample and before it in the other.

Characterization

TG experiment was carried out with a TA Instruments SDT 2960 machine, with a heating rate of 10 °C min⁻¹ until 550 °C and flow rate of 130 cm³ min⁻¹ air simulating the environment during the removal of the polystyrene nanospheres. To gain sample, the polystyrene nanospheres of an opal were scraped off and filled into the TG sample holder.

The SEM images were taken with a LEO 1540 XB scanning electron microscope, in high vacuum mode and using the secondary electron detector. The samples were hold in place with adhesive carbon tapes on top of the copper sample holder. For better image quality of the polystyrene and carbon opals the samples were sputtered an Au/Pd layer.

EDX spectra were taken by JEOL JSM-5500LV scanning electron microscope, for each sample three measurement points were averaged.

XRD measurement of the inverse opal samples were made by PANanalytical X'Pert Pro MPD X-ray diffractometer using Cu K- α radiation, between the angle range of 5°–65°.

The reflectance UV–Vis spectra were also recorded by a Avantes AvaSpec-2048 spectrophotometer equipped with optical cables and Si wafer as reference.

UV–Vis reflectance spectrum was recorded by Avantes AvaSpec-2048 spectrophotometer equipped with optical cables, and the substrate Si wafers were used as reference.

Results and discussion

The synthesis paths (Fig. 1) shows that the first step was the preparation of the colloid crystal using vertical deposition. The colloid crystal was filled with ZnO using DEZ and H₂O precursors. The synthesis was continued in two

different courses: growth of ZnO nanorods using hydrothermal synthesis and then remove the polystyrene colloid crystal template (Fig. 2a), removing the template before the growth of ZnO nanorods. The two-path provided different structures, one with more plate like forms (A) and one with nanorods (B). The second structure were investigated more thoroughly, since its closer in morphology to an inverse opal/nanorod hybrid structure.

The polystyrene nanospheres were taken from an opal sample and filled into the TG sample holder. Based on the TG curve (Fig. 2), a minor mass loss occurs between 100 and 300 °C, where it loses 2.45% of its mass and a major

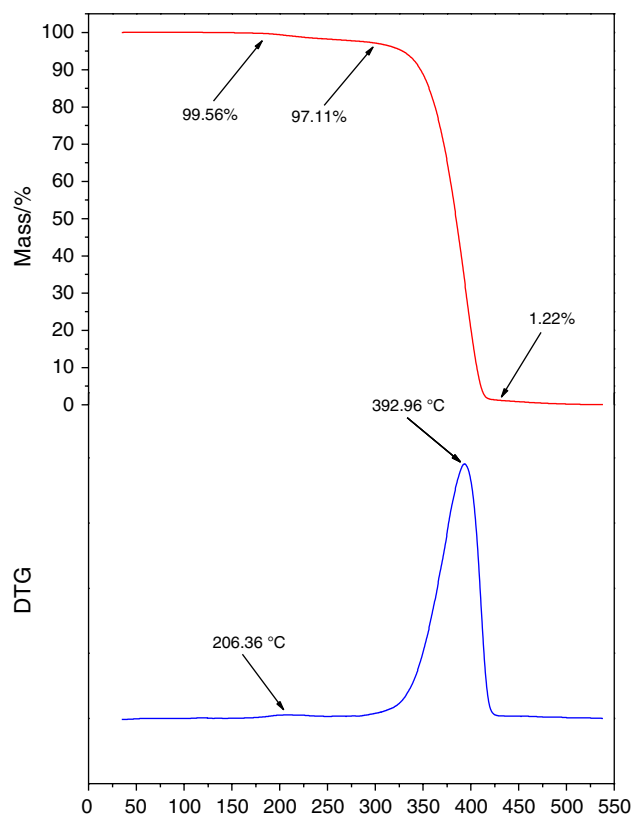


Fig. 2 TG analysis of the polystyrene nanospheres in air

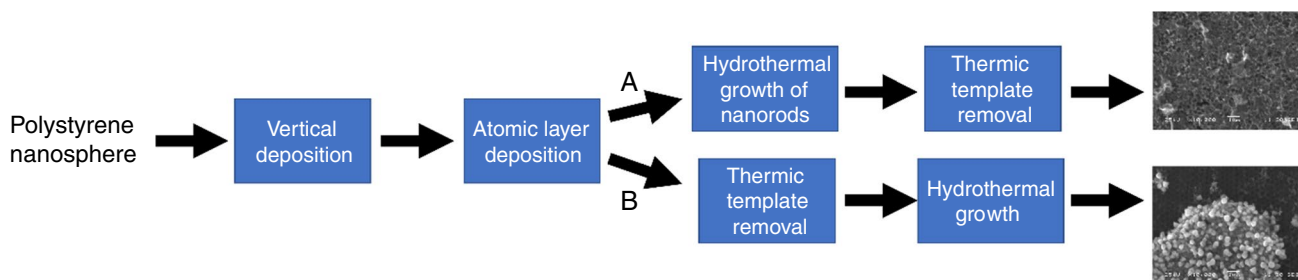


Fig. 1 The synthesis paths of the hybrid structures: hydrothermal growth of nanorods before template removal (a) and hydrothermal growth of nanorods after template removal (b)

between 300 and 425 °C, where it loses 95.89% of its mass. These two events are reinforced by the DTG curve where around ~206 °C is a flat peak and at ~393 °C. According to literature the first drop in mass is the departure of water and polystyrene monomers from the system and the second event is the decomposition of polystyrene [44]. Therefore, 500 °C was suitable as annealing temperature to remove the sacrificial polystyrene nanospheres to obtain the ZnO inverse opals.

SEM images of Fig. 3a show the hexagonally ordered opal structure prepared from 460 nm polystyrene nanospheres. This opal served as the template for the inverse opal reference and for the hybrid inverse opal/nanorod samples. In Fig. 3b, the reference inverse opal is observable, and it has the same hexagonal structure as the opal. In Fig. 3c, the reference ZnO nanorod forest is presented, and the average diameter of the nanorods is around ~300 nm. In Fig. 2d, e, two inverse opal/nanorod samples show different structures. The removal of the polystyrene nanospheres only after the hydrothermal growth gives a layer of plate like structures and the inverse opal structure is still observable (Fig. 3d). Removing the polystyrene nanospheres before the hydrothermal growth created a ZnO nanorod forest with a different structure than the reference (Fig. 3e). Possibly, this difference is caused by the bumpy surface of the inverse opal. It's also observable that these nanorods did not grow on the entire surface of the inverse opal. From this point on we investigated the more organized structure.

The composition of the references samples was measured with EDX (Table 1). In both cases Zn and O were detected

Table 1 Composition of the two reference samples

Element	w/w%	
	ZnO nanorod forest	ZnO inverse opal
C	4.6	–
O	9.2	14.8
Al	3.5	2.5
Si	1.8	63.3
Zn	81.0	19.5

indicating the presence of ZnO. The signal Si is coming from the substrate slide. The ZnO nanorod layer was thicker than the hollow inverse opal structure; thus here the Si signal was weaker. On the other hand, there is a detectable amount of C in the nanorod forest, which is probably from the residual hexamethylene-tetramin and Zn-acetate. This also shows that the polystyrene nanospheres were successfully removed with the annealing, as no C was detected in the inverse opal. Al is probably from the sample holder of the SEM.

The crystallinity of the samples was determined using XRD. The diffractogram of the Si wafer was recorded to distinguish its peaks from the samples (Fig. 4a). Grown ZnO structures such as the nanorods, inverse opal and the structure of the hybrid samples all proved to be wurtzite ZnO (Fig. 4b–d). The reference ZnO nanorod forest sample has intense Si peaks that belonged to the substrate, thus to check the presence of ZnO, a zoomed image is shown in the inset (Fig. 4b). The diffractograms of the inverse opal and the hybrid structure (Fig. 4c, d) are basically identical.

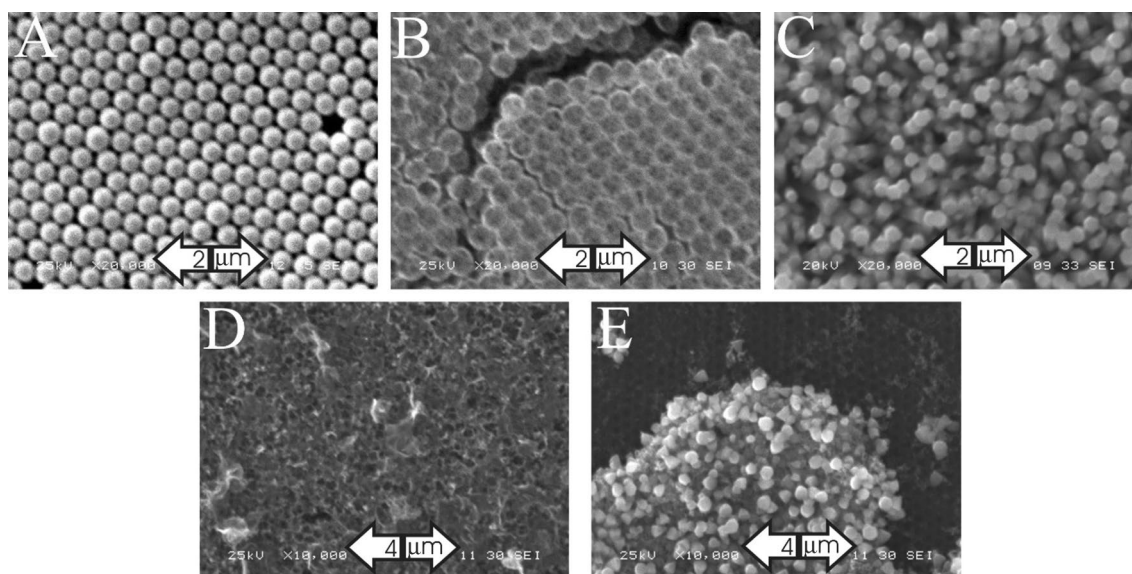


Fig. 3 SEM image of the 460 nm polystyrene opal crystal template (a), ZnO inverse opal reference (b), ZnO nanorod forest (c), the ZnO inverse opal/nanorod hybrid with the polystyrene nanospheres

removed after the hydrothermal growth (d) and the ZnO inverse opal/nanorod hybrid with the polystyrene nanospheres removed before the hydrothermal growth (e)

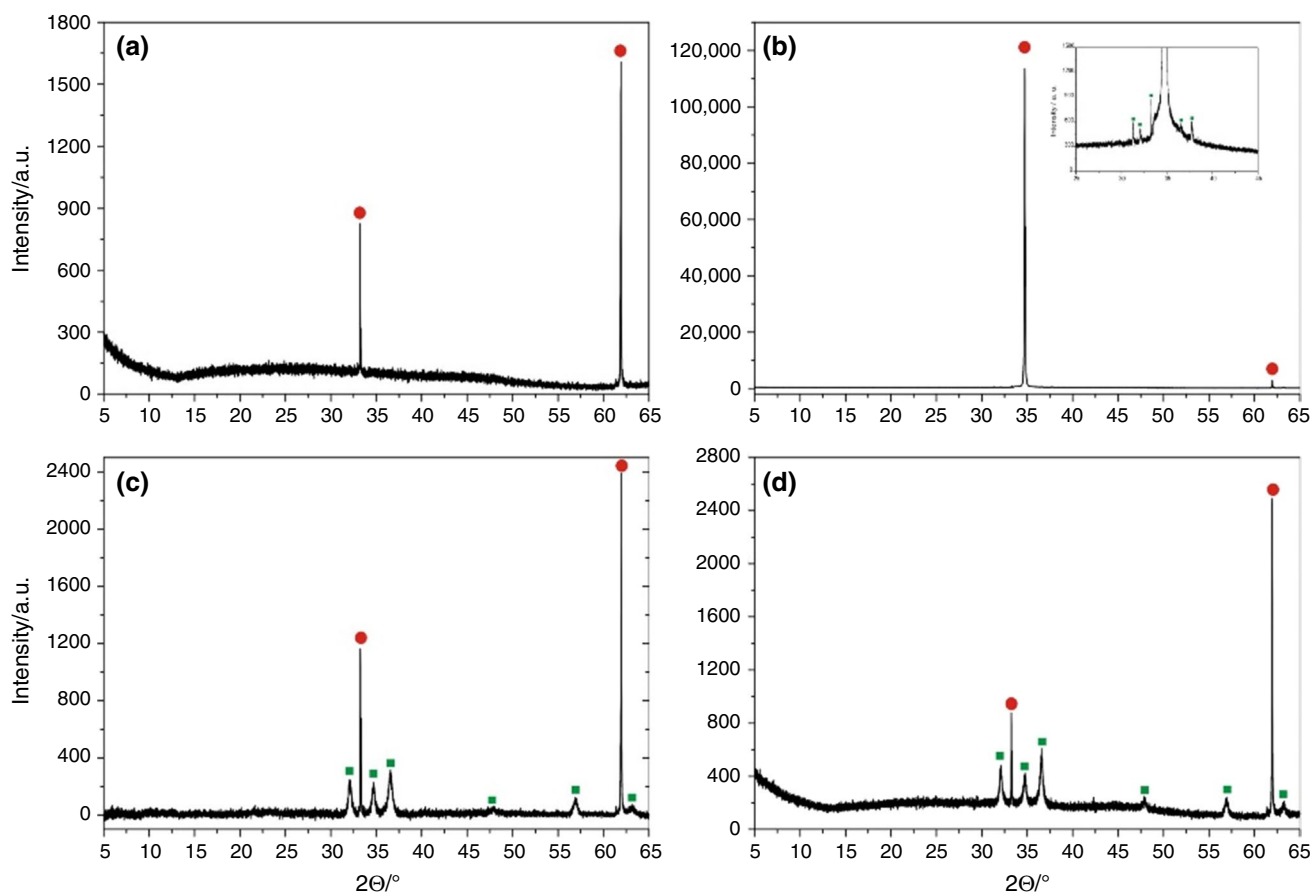


Fig. 4 X-ray diffractograms of the Si wafer substrate (a), ZnO nanorod forest reference (b), ZnO inverse opal reference (c) and the inverse opal/nanorod hybrid sample with the polystyrene removed

before the hydrothermal growth (d). Red circle signal from the Si wafer substrate, green square signal from the wurtzite ZnO [45]

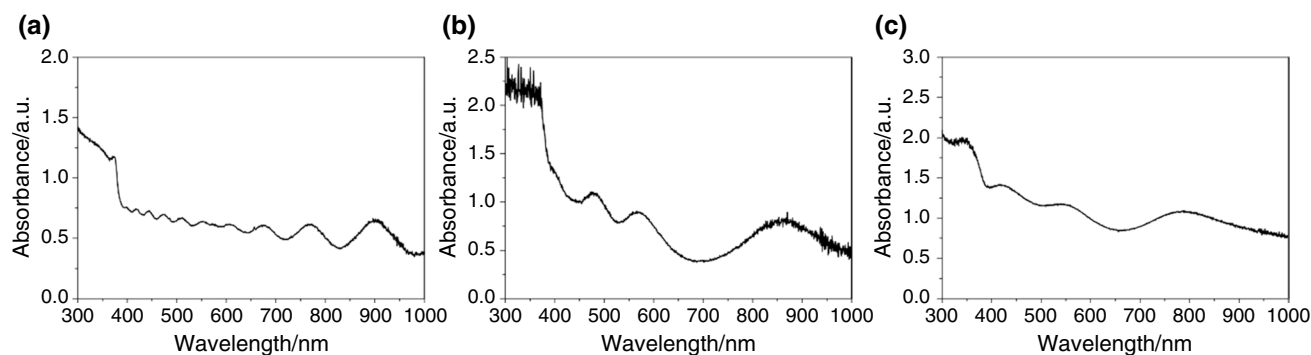


Fig. 5 UV–Vis absorbance spectra of the ZnO nanorod forest reference (a), the ZnO inverse opal (b) and the inverse opal/nanorod hybrid sample with the polystyrene removed before the hydrothermal growth (c)

The three UV–Vis spectra (Fig. 5) all have the typical absorption edge of the ZnO semiconductor, which is usually between 350 and 400 nm [43]. The ZnO nanorod forest reference has multiple absorption peaks (Fig. 5a), this sinusoidal absorption pattern is corresponding to the several μm thick layer. The ZnO inverse opal reference (Fig. 5b) has three

absorption peaks (475 nm, 565 nm and 860 nm), for inverse opals with these structure (polystyrene size—460 nm) has a photonic band gap at the visible light range, this is observable at 525 nm and the two “slow” photon absorption enhancement at 475 nm and 565 nm. For the hybrid structure the spectra (Fig. 5c) is similar, the three absorption peaks

(420 nm, 540 nm and 775 nm). The photonic band gap is around 500 nm and the two absorption peaks next to it at 420 nm and 520 nm. This might be caused that small hydrothermal growth of ZnO might have happened not only on the surface of the inverse opal, but also inside it and this few nm hydrothermal ZnO layer on the ALD ZnO walls narrowed a few nm the diameter of the air voids.

Conclusions

In this study, we explored the combination of the synthesis of a ZnO inverse opal by ALD and vertical deposition with the hydrothermal growth of ZnO nanorods. Hydrothermal growth was done before and after the thermal removal of the polystyrene opal template to check the effect of annealing, resulting in two different structures. SEM images revealed that the former route provided a less organized, plate like ZnO structure on the surface of the inverse opal. The cause of this might be both the presence of the polystyrene nanospheres and the absence of annealing. The latter route gave a nanorod forest on top of the inverse opal with an increasing diameter to the top of nanorods, i.e. looking like reversed cones. This is probably caused by the surface geometry of the inverse opal as substrate. In earlier works usually an extra seed layer was deposited on the surface of the inverse opal or the diameter of the nanorods were significantly smaller than the void holes of the hollow structure. From this point on we investigated the more organized structure. EDX and X-ray diffractograms both proved that the sample was made of wurzite ZnO and that the polystyrene nanospheres were successfully removed after the annealing. UV–Vis spectroscopic studies showed that the inverse opal reference has photonic band gap at ~520 nm and that the hybrid structure has it at ~500 nm. The difference between the two structures can be explained either by the hydrothermally grown structure on the surface of the inverse opal or the hydrothermal growth slightly modified the inner parts of the hollow structure, like decreasing the size of the void holes, which can shift the photonic band gap.

Acknowledgements An NRD K 124212 and an NRD TNN_16 123631 grants are acknowledged. The research within project No. VEKOP-2.3.2-16-2017-00013 was supported by the European Union and the State of Hungary, co-financed by the European Regional Development Fund. The research reported in this paper and carried out at BME has been supported by the NRD Fund TKP2021 BME-NVA based on the charter of bolster issued by the NRD Office under the auspices of the Ministry for Innovation and Technology. The research was supported by the Thematic Excellence Programme (TKP2020-IKA-04) of the Ministry for Innovation and Technology in Hungary.

Funding Open access funding provided by Budapest University of Technology and Economics.

Open Access This article is licensed under a Creative Commons Attribution 4.0 International License, which permits use, sharing, adaptation, distribution and reproduction in any medium or format, as long as you give appropriate credit to the original author(s) and the source, provide a link to the Creative Commons licence, and indicate if changes were made. The images or other third party material in this article are included in the article's Creative Commons licence, unless indicated otherwise in a credit line to the material. If material is not included in the article's Creative Commons licence and your intended use is not permitted by statutory regulation or exceeds the permitted use, you will need to obtain permission directly from the copyright holder. To view a copy of this licence, visit <http://creativecommons.org/licenses/by/4.0/>.

References

1. Armstrong E, O'Dwyer C. Artificial opal photonic crystals and inverse opal structures – fundamentals and applications from optics to energy storage. *J Mater Chem C R Soc Chem*. 2015;3:6109–43.
2. Jovic V, Idriss H, Waterhouse GIN. Slow photon amplification of gas-phase ethanol photo-oxidation in titania inverse opal photonic crystals. *Chem Phys*. 2016;479:109–21. <https://doi.org/10.1016/j.chemphys.2016.10.001>.
3. Chen JIL, von Freymann G, Choi SY, Kitaev V, Ozin GA. Slow photons in the fast lane in chemistry. *J Mater Chem*. 2008;18:369–73.
4. Zheng X, Meng S, Chen J, Wang J, Xian J, Shao Y, et al. Titanium dioxide photonic crystals with enhanced photocatalytic activity: matching photonic band gaps of TiO₂ to the absorption peaks of dyes. *J Phys Chem C*. 2013;117:21263–73. <https://doi.org/10.1021/jp404519j>.
5. Zhang X, John S. Enhanced photocatalysis by light-trapping optimization in inverse opals. *J Mater Chem A*. 2020;8:18974–86.
6. Huang X, Chen J, Lu Z, Yu H, Yan Q, Hng HH. Carbon inverse opal entrapped with electrode active nanoparticles as high-performance anode for lithium-ion batteries. *Sci Rep*. 2013;3.
7. Liu L, Karuturi SK, Su LT, Tok AIY. TiO₂ inverse-opal electrode fabricated by atomic layer deposition for dye-sensitized solar cell applications. *Energy Environ Sci*. 2011;4:209–15.
8. Fenzl C, Hirsch T, Wolfbeis OS. Photonic crystals for chemical sensing and biosensing. *Angew. Chemie - Int. Ed*. 2014.
9. Geng C, Wei T, Wang X, Shen D, Hao Z, Yan Q. Enhancement of light output power from LEDs based on monolayer colloidal crystal. *Small*. 2014.
10. Xu Y, Schneider GJ, Wetzel ED, Prather DW. Centrifugation and spin-coating method for fabrication of three-dimensional opal and inverse-opal structures as photonic crystal devices. *J Microlithogr Microfabr Microsystems*. 2004;3.
11. Zhou Z, Zhao XS. Opal and inverse opal fabricated with a flow-controlled vertical deposition method. *Langmuir*. 2005;21.
12. Benoit F, Dieudonné E, Bertussi B, Vallé K, Belleville P, Mallejac N, et al. Development of 3D photonic crystals using sol-gel process for high power laser applications. *Nanoeng Fabr Prop Opt Devices XII*. 2015.
13. Romanov SG, Johnson NP, Fokin A V., Butko VY, Yates HM, Pemble ME, et al. Enhancement of the photonic gap of opal-based three-dimensional gratings. *Appl Phys Lett. American Institute of Physics Inc.*; 1997;70:2091–3.
14. Braun P V., Wiltzius P. Macroporous materials: electrochemically grown photonic crystals. *Curr Opin Colloid Interface Sci. Nature Publishing Group*; 2002;7:116–23.

15. King JS, Graugnard E, Summers CJ. TiO₂ inverse opals fabricated using low-temperature atomic layer deposition. *Adv Mater*. 2005;17:1010–3.
16. Scharrer M, Wu X, Yamilov A, Cao H, Chang RPH. Fabrication of inverted opal ZnO photonic crystals by atomic layer deposition. *Appl Phys Lett*. 2005;86.
17. Rügge A, Becker JS, Gordon RG, Tolbert SH. Tungsten nitride inverse opals by atomic layer deposition. *Nano Lett*. 2003;3:1293–7.
18. George SM. Atomic layer deposition: an overview. *Chem Rev*. 2010;110:111–31.
19. Yu J, Lei J, Wang L, Zhang J, Liu Y. TiO₂ inverse opal photonic crystals: synthesis, modification, and applications: a review. *J Alloys Compd*. 2018; p. 740–57.
20. Long J, Fu M, Li C, Sun C, He D, Wang Y. High-quality ZnO inverse opals and related heterostructures as photocatalysts produced by atomic layer deposition. *Appl Surf Sci*. 2018;454.
21. Schroden RC, Al-Daous M, Blanford CF, Stein A. Optical properties of inverse opal photonic crystals. *Chem Mater*. 2002;14:3305–15.
22. Liu FT, Gao SF, Pei SK, Tseng SC, Liu CHJ. ZnO nanorod gas sensor for NO₂ detection. *J Taiwan Inst Chem Eng*. 2009;40:528–32.
23. Kuehnel MF, Creissen CE, Sahm CD, Wielend D, Schlosser A, Orchard KL, et al. ZnSe nanorods as visible-light absorbers for photocatalytic and photoelectrochemical H₂ evolution in water. *Angew Chemie - Int Ed*. 2019;58:5059–63.
24. Aspoukeh PK, Barzinjy AA, Hamad SM. Synthesis, properties and uses of ZnO nanorods: a mini review. *Int Nano Lett*. 2021;
25. Perillat-Merceroz G, Jouneau H, Feuillet G, Thierry R, Rosina M, Ferret P. MOCVD growth mechanisms of ZnO nanorods. *J Phys Conf Ser*. 2010.
26. Poornajar M, Marashi P, HaghshenasFatmehsari D, Kolahdouz EM. Synthesis of ZnO nanorods via chemical bath deposition method: the effects of physicochemical factors. *Ceram Int*. 2016;42:173–84.
27. Liu B, Zeng HC. Hydrothermal synthesis of ZnO nanorods in the diameter regime of 50 nm. *J Am Chem Soc*. 2003;125:4430–1.
28. Gerbreder V, Krasovska M, Sledzskis E, Gerbreder A, Mihailova I, Tamanis E, et al. Hydrothermal synthesis of ZnO nanostructures with controllable morphology change. *CrystEngComm*. 2020;22:1346–58.
29. Kozhummal R, Yang Y, Güder F, Hartel A, Lu X, Küçükbayrak UM, et al. Homoepitaxial branching: An unusual polymorph of zinc oxide derived from seeded solution growth. *ACS Nano*. 2012;6.
30. Yang Y, Wang H, Cai Y, Wang C, Xu H, Fang J. Seeded growth of ZnO nanowires in dye-containing solution: The submerged plant analogy and its application in photodegradation of dye pollutants. *CrystEngComm*. 2020;22.
31. Li D, Hu J, Low ZX, Zhong Z, Wang Y. Hydrophilic ePTFE membranes with highly enhanced water permeability and improved efficiency for multipollutant control. *Ind Eng Chem Res*. 2016;55.
32. Turberfield a. J. Fabrication of photonic crystals for the visible spectrum by holographic lithography. *Nature*. 2000;404:53–6.
33. Liu J, Liu G, Li M, Shen W, Liu Z, Wang J, et al. Enhancement of photochemical hydrogen evolution over Pt-loaded hierarchical titania photonic crystal. *Energy Environ Sci*. 2010;3:1503–6.
34. Karuturi SK, Cheng C, Liu L, Tat SuL, Fan HJ, Tok AIY. Inverse opals coupled with nanowires as photoelectrochemical anode. *Nano Energy*. 2012;1:322–7.
35. Park Y, Lee JW, Ha SJ, Moon JH. 1D nanorod-planted 3D inverse opal structures for use in dye-sensitized solar cells. *Nanoscale*. 2014;6:3105–9.
36. Zheng XL, Qin WJ, Ling T, Pan CF, Du XW. Carbon nanotube reinforced CdSe inverse opal with crack-free structure and high conductivity for photovoltaic applications. *Adv Mater Interfaces*. 2015;2.
37. Jang YJ, Lim J, Kim SO, Kim DH. Carbon nanotube-grafted inverse opal nanostructures. *Opt Mater Express*. 2017;7.
38. Boppella R, Kochuveedu ST, Kim H, Jeong MJ, Marques Mota F, Park JH, et al. Plasmon-sensitized graphene/TiO₂ inverse opal nanostructures with enhanced charge collection efficiency for water splitting. *ACS Appl Mater Interfaces*. 2017;9.
39. Zulfiqar A, Temerov F, Saarinen JJ. Multilayer TiO₂ inverse opal with gold nanoparticles for enhanced photocatalytic activity. *ACS Omega*. 2020;5:11595–604.
40. Labouchere P, Chandiran AK, Moehl T, Harms H, Chavhan S, Tena-Zaera R, et al. Passivation of ZnO nanowire guests and 3D inverse opal host photoanodes for dye-sensitized solar cells. *Adv Energy Mater*. 2014;4.
41. Giancaterini L, Cantalini C, Cittadini M, Sturaro M, Guglielmi M, Martucci A, et al. Au and Pt nanoparticles effects on the optical and electrical gas sensing properties of sol-gel-based ZnO thin-film sensors. *IEEE Sens J*. 2015;15:1068–76.
42. Bakos LP, Karajz D, Katona A, Hernadi K, Parditka B, Erdélyi Z, et al. Carbon nanosphere templates for the preparation of inverse opal titania photonic crystals by atomic layer deposition. *Appl Surf Sci*. 2020;504.
43. Russell JL, Noel GH, Warren JM, Tran NLL, Mallouk TE. Binary colloidal crystal films grown by vertical evaporation of silica nanoparticle suspensions. *Langmuir*. 2017;33:10366–73.
44. Loiola AR, Da Silva LRD, Cubillas P, Anderson MW. Synthesis and characterization of hierarchical porous materials incorporating a cubic mesoporous phase. *J Mater Chem*. 2008;18.
45. Yedurkar S, Maurya C, Mahanwar P. Biosynthesis of zinc oxide nanoparticles using *Ixora Coccinea* leaf extract: a green approach. *Open J Synth Theory Appl*. 2016;05.

Publisher's Note Springer Nature remains neutral with regard to jurisdictional claims in published maps and institutional affiliations.